Thermophoretic transport of ionic liquid droplets in carbon nanotubes

Rajegowda, Rakesh; Kannam, Sridhar Kumar; Hartkamp, Remco; Sathian, Sarith P.

Important note
To cite this publication, please use the final published version (if applicable).
Please check the document version above.

Thermophoretic transport of ionic liquid droplets in carbon nanotubes

Rakesh Rajegowda

Department of Applied Mechanics, Indian Institute of Technology Madras, Chennai 600036, India.

E-mail: `r.rakzz@gmail.com`

Sridhar Kumar Kannam

IBM Research Australia, 204 Lygon Street, 3053 Carlton, Victoria, Australia.

E-mail: `urssrisri@gmail.com`

Remco Hartkamp

Process and Energy Department, Delft University of Technology, Leeghwaterstraat 39, 2628 CB Delft, The Netherlands

E-mail: `remcohartkamp@gmail.com`

Sarith P. Sathian

Department of Applied Mechanics, Indian Institute of Technology Madras, Chennai 600036, India.

E-mail: `sarith@iitm.ac.in`

Abstract. Thermal-gradient induced transport of ionic liquid (IL) and water droplets through a carbon nanotube (CNT) is investigated in this study using molecular dynamics simulations. Energetic analysis indicates that IL transport through a CNT is driven primarily by the fluid-solid interaction, while fluid-fluid interactions dominate in water-CNT systems. Droplet diffusion analysis via the Moment Scaling Spectrum reveals sub-diffusive motion of the IL droplet, in contrast to the self-diffusive motion of the water droplet. The Soret coefficient and energetic analysis of the systems suggest that the CNT shows more affinity for interaction with IL than with the water droplet. Thermophoretic transport of IL is shown to be feasible, which can create new opportunities in nanofluidic applications.

1. Introduction

The rapid emergence of nanofluidic devices for health, energy, and environment, urges the development of an improved fundamental understanding of fluid and nanoparticle transport in nanoconfinement [1, 2]. Transport through carbon nanotubes (CNTs) has

received special attention over the past two decades due to the unique mechanical, electrical and chemical properties of CNTs; for example that they can act as a metal or a semiconductor depending on their diameter and chirality [3]. The interest in CNTs is further fueled by their usage as a model for studying mass transport through quasi-one-dimensional channels for drug delivery [4], molecular filtration and separation, and electro-chemical energy storage [5]. Mass transport at the nanoscale can be driven by various mechanical, thermodynamical and chemical forces, such as a thermal gradient [6, 7, 8], electric potential (electrophoresis and electroosmosis) [9, 10], concentration [11], pressure [12], or surface tension (Marangoni effect) [11].

The effect of thermal gradient on fluid properties was first reported by Ludwig [13] in 1856, who found density and concentration variations in a salt solution at a non-uniform temperature. This phenomenon was later investigated by Soret [14], who observed a non-uniform salt concentration in a confined aqueous solution subjected to a thermal gradient. Based on molecular-level interactions, Maxwell [15] proposed a physical basis for a driving force that induces a flow due to non-uniform temperature. Such variations were later found to drive fluids or immersed particles to flow against the direction of a temperature gradient. This became the basis of thermophoresis (also known as thermodiffusion and the Soret effect) [15], in which the transport is induced by a thermophoretic driving force F_{th} resulting from a thermal gradient. Confined fluids exchange momentum and energy with the solid walls through collisions, absorption, and desorption. Subjecting the wall surface to a temperature gradient causes spatial variations in the average momentum of wall atoms and in the exchange of momentum and energy with interfacial fluid. Consequently, a net force, due to the thermal gradient applied, drives the fluid from the hot to the cold end of the system.

The majority of research on thermophoretic flow has been focused on rarefied gases [16, 17, 18, 19, 20], for which extensive theoretical models have been developed. For example, Ibbs [18, 19] found that the thermal diffusion coefficient of various gases was more sensitive to intermolecular forces than the transport coefficients. In addition to gas flow, various recent studies have focused on the transport of droplets [21], nanoparticles [22], fullerene [23] and short CNTs along the outer surface of longer CNTs [24, 25, 26, 27, 28]. The latter case deviates from a fluid-based transport mechanism since a phonon current between the inner and outer tube is the dominant driving force, rather than a momentum exchange between atoms. The present work is focused on thermodiffusion of fluid droplets, hence the possibility of phonon current is not further discussed here. Molecular dynamics (MD) simulations have been instrumental in elucidating and predicting fluid motion induced by a thermal gradient. For example, Zambrano *et al* [21] demonstrated via MD simulations that thermal diffusion occurs both in the translational and rotational motion of water (W) nanodroplets in a CNT, with the streaming motion guided by the helical angle of the tube. The thermal gradient applied in axial direction has a weak influence on the surface wettability, while it has a strong influence on the isothermal diffusion. Hence the Soret coefficient, the ratio of thermal and isothermal diffusion coefficients, is altered by the
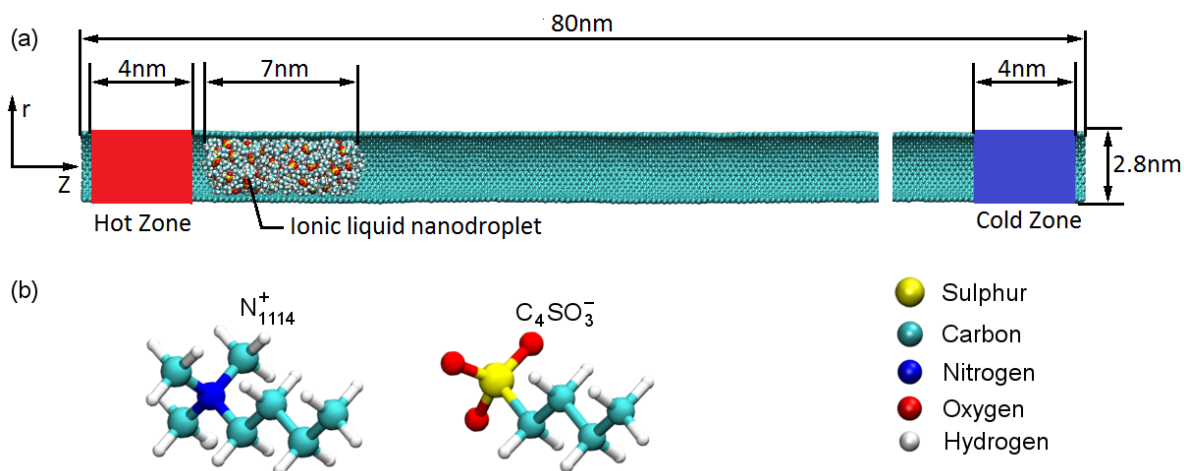
applied thermal gradient [21].

Figure 1. (a) Cross-section view of the ionic liquid inside a CNT. A thermal gradient is imposed by thermostatting the hot and cold regions (shown in red and blue). (b) The molecular structure of 1-butyl-1,1,1-methylammonium cation (N_{1114}^{+}) and butane sulfonate anion ($C_4SO_3^{-}$) ions.

Shiomi and Maruyama [29] estimated, for a similar system as the one studied by Zambrano *et al* [21], the thermophoretic force acting on a droplet and suggested that the potential energy of W-W interactions is sufficient to drive the droplet through the CNT. A thermal gradient as low as 0.18 K/nm was sufficient to transport a water nanodroplet through a CNT. The thermophoretic forces acting on the droplet and the potential energy due to W-W and W-CNT interactions varied linearly with the applied thermal gradient. They also demonstrated that sudden variations in the tube diameter along its axis cause a disturbance in the droplet motion, due to irregularities in the trajectories of the molecules. Rurali and Hernandez [30] investigated the viability of fullerene transport via thermophoresis and its sensitivity to the nanotube wall structure (chirality). Most fluids, including water, have a narrow window of thermal and electrical stability, limiting their usability in applications under extreme conditions. Conversely, room temperature ionic liquids (RTILs) have shown much promise in energy and heat transfer applications because they are nonflammable, nonvolatile, thermally stable, have a high electrical conductivity, and are liquids under a wide range of temperatures [31]. RTILs have gained popularity in recent years because they are considered as a green alternative to organic solvents for chemical synthesis [32]. As such, RTILs are potential candidates for use in electrochemical devices such as batteries [33], supercapacitors [5], fuel cells [34] and solar cells [35]. Accurately transporting these highly viscous fluids through a nanoconfined environment via a mechanical driving force is challenging. On the other hand, temperature gradients can be induced for example by irradiating the tube ends via continuous or pulsating electron beams [25]. Thermophoretic transport of nanoconfined IL has not yet been investigated to our knowledge, this type of transport may be very appropriate for thermally stable fluids such as ILs. In the present study, the

thermophoretic transport of an ionic liquid droplet through a single-walled CNT (shown in Fig. 1(a)) is investigated via MD simulation.

2. Methodology

The simulated system is an ionic liquid droplet confined inside an armchair CNT (21,21) of diameter 2.8 nm and length 80 nm, see Fig. 1(a). The droplet, which consists of 60 ion pairs, is approximately 7 nm long. Thermophoresis is investigated by imposing a temperature gradient between 1 K/nm and 6 K/nm along the axial tube direction. We consider 1-butyl-1,1,1-methylammonium cation (N_{1114}^+) and butane sulfonate anion ($C_4SO_3^-$), which are environmentally friendly in comparison to other commonly studied RTILs [37]. Following prior thermophoretic simulations [29, 21], 1 nm at both ends of the CNT is kept rigid, such that no momentum is exchanged between the high and low temperature sides of the tube via the periodic boundary. Additionally, the constraint on the tube ends avoids potential drifting and bending of the CNT. A series of steps are performed to ensure the equilibration of the system. Following an energy minimization, the system is equilibrated at 300 K for 1.5 ns, during which the ions form a liquid droplet. The droplet is then moved to the left end (hot side) of the tube by connecting the centre of mass of the droplet to a spring centered at 10 nm from the tube end and continuing the simulation for 0.5 ns in a microcanonical ensemble (i.e., the temperature is not explicitly controlled during this stage). The energy of the droplet is monitored to confirm convergence. Finally, Nosé-Hoover thermostats are applied to the wall atoms in the 4 nm next to the rigid ends, with a hot T_h and a cold T_c side to impose a temperature gradient ($T_h > T_c$) in the axial direction. The temperature of the cold end of the CNT is kept at 300 K (T_c), while the hot end has a higher temperature (T_h), between 370 to 720 K, to obtain a thermal gradient of 1 to 6 K/nm, respectively. The system is equilibrated for an additional 0.5 ns, amounting to a total equilibration time of 2.5 ns. Once the simulation system is equilibrated, the constraint on the centre of mass of the IL droplet is removed and thermophoretic transport occurs. The production run lasted for as long as needed for the IL droplet to cross the CNT, which varied between 0.5 ns for the largest thermal gradient, to 6.6 ns for the smallest one.

Simulations were performed with the LAMMPS [36] simulation package, with a timestep of 2 fs. Ionic liquid interactions were described by the all-atom force field parameters of Lopes *et al* [37] in which the functional form of bonded interaction are based on the OPLS-AA force field and non-bonded interactions on the CHARMM force field, with a damping between the inner (12 Å) and the outer cutoff radius (14 Å) [38]. Carbon-carbon interactions in the CNT were described by the REBO Potential [39], which is a reactive bond-order potential that has been used widely [40, 41, 28] for calculating thermal transport properties of carbon-based materials. The Lorentz-Berthelot mixing rule was used to model interactions between the liquid and the CNT.

3. Results and discussions

Thermophoretic forces on the droplet are measured under the influence of six different thermal gradients varying linearly from 1 to 6 K/nm. While thermal gradients used in experiments are typically smaller than 1 K/nm [24], larger gradients are needed in molecular simulation to obtain a large signal-to-noise ratio. Simulations at each thermal gradient are carried out five times to further improve the statistics, with each simulation having different random initial velocities.
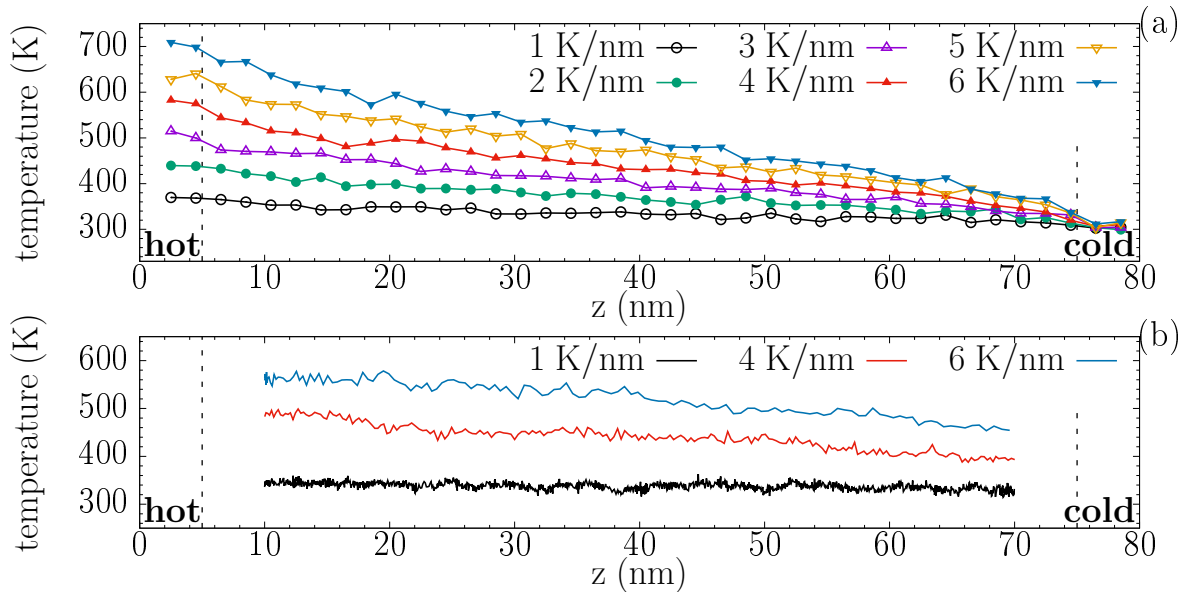

Figure 2. The temperature of (a) CNT measured along its length and (b) IL as it transported through tube at various thermal gradients

Fig. 2(a) shows the CNT temperature along its length, measured in bins of width 0.2 nm. The non-linear temperature profile indicates a non-Fourier heat conduction behavior, consistent with the literature [28, 20, 41, 42]. Figs. 2(b) shows the temperature variation of the IL droplet as it is transported through the CNT for thermal gradients of 1, 4 and 6 K/nm. The interaction energy between IL and CNT ($E_{\text{IL−CNT}}$) as the droplet move from the hot to the cold region is shown in Fig. 3(a). The droplet minimizes its interaction energy with the nanotube as it moves towards the colder region. Adaptive Biasing Force (ABF) simulations [44] are carried out to evaluate the potential of mean force (PMF) and to measure the free energy that the droplet gains when moving towards the colder region. The PMF is measured by dividing the tube into 30 windows of 2 nm each. As can be seen in Fig. 3(b): (i) The 1-dimensional energy landscape is simple; it varies linearly with the temperature gradient along the axial direction of the tube. (ii) The gradient in PMF increases with increasing temperature gradient on the tube. (iii) For temperature gradients of 1, 4 and 6 K/nm, the droplet gains, respectively, 67.03, 236.54 and 371.90 kJ/mol free energy by moving from hot to the cold region.

Figs. 4(a) and (b) show, respectively, the centre-of-mass velocity (v_{cm}) and the force
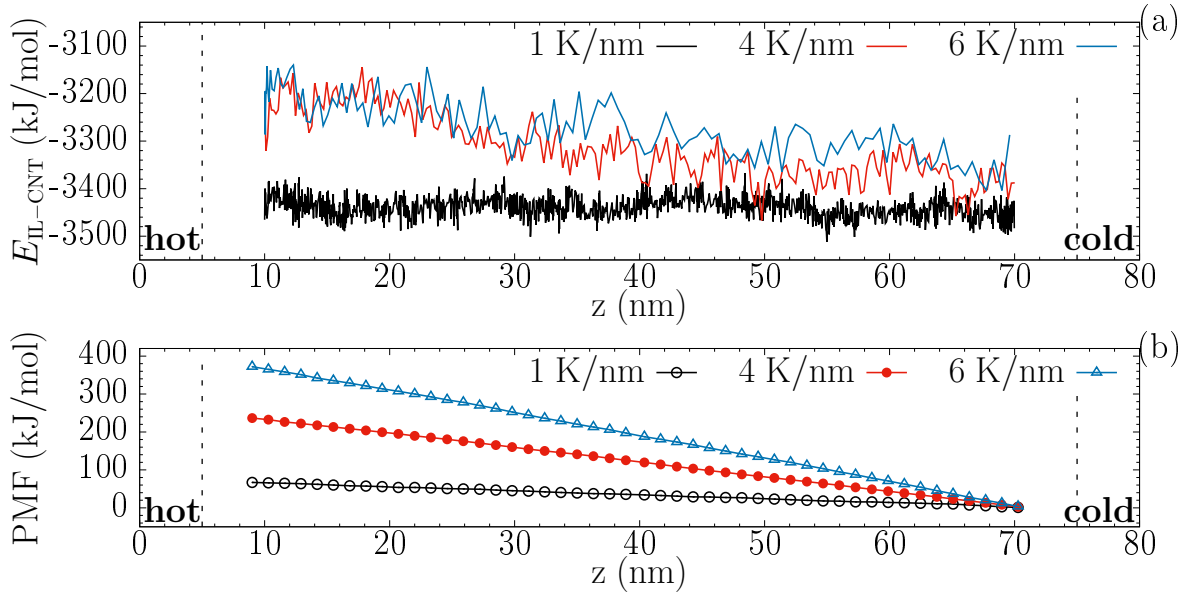
Figure 3. (a) Interaction potential energy of between the droplet and CNT as the droplet move from hotter to colder region along the nanotube axis. (b) Potential of mean force of the droplet against its centre-of-mass position.
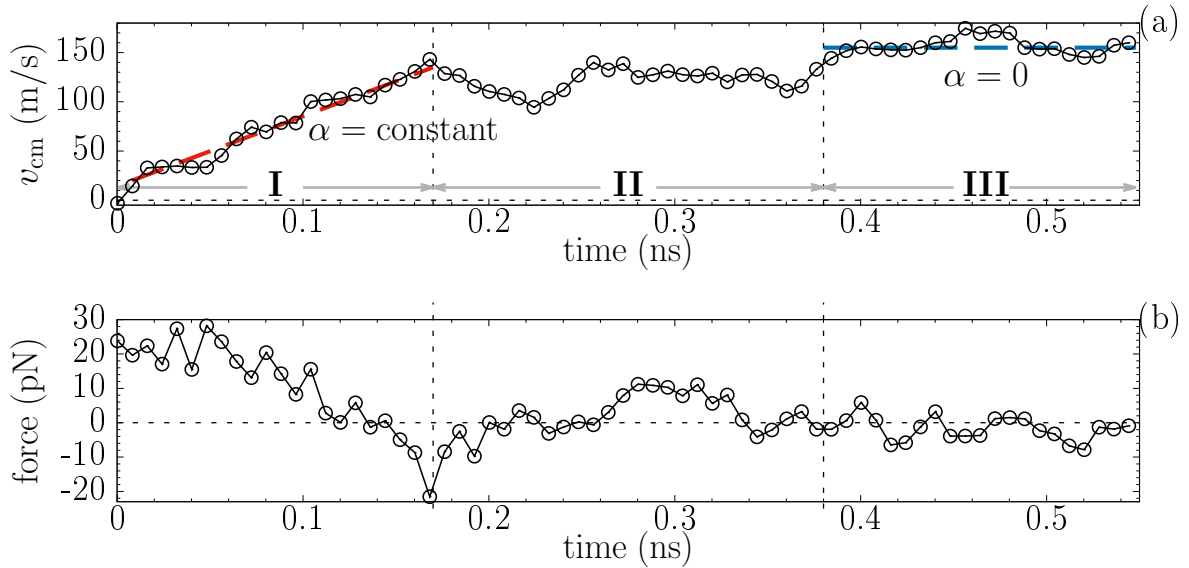

Figure 4. Change in (a) the velocity of centre of mass of droplet and (b) force acting on IL droplet over time. Region I, II and III (in (a)) show the acceleration phase with a constant slope (α), transient phase and steady phase with a constant speed, respectively.

acting on the droplet as a function of time, at 6 K/nm thermal gradient. The droplet travels from the hot end (10 nm) to the cold end (70 nm) in 0.548 ns, during which the temperature of the droplet drops from 560 to 450 K, as was shown in Fig. 3(a). This shows that the time spent by the droplet at any position along the tube axis is too

small to relax to the local tube temperature. The transport of the droplet through the nanotube is divided into three phases based on its velocity, as shown in Fig. 4(a). In phase-I the droplet shows a near-constant acceleration, followed by a transient phase-II, in which frictional forces might provide resistance to the flow, eventually causing a steady flow phase-III in which the thermophoretic and frictional forces are balanced and the droplet reaches a terminal velocity of 155 m/s. Fig. 4(b) shows the total force acting on the droplet, which is dominated by the thermophoretic force at phase-I and slowly reduces to an average force of zero in phases-II and III.
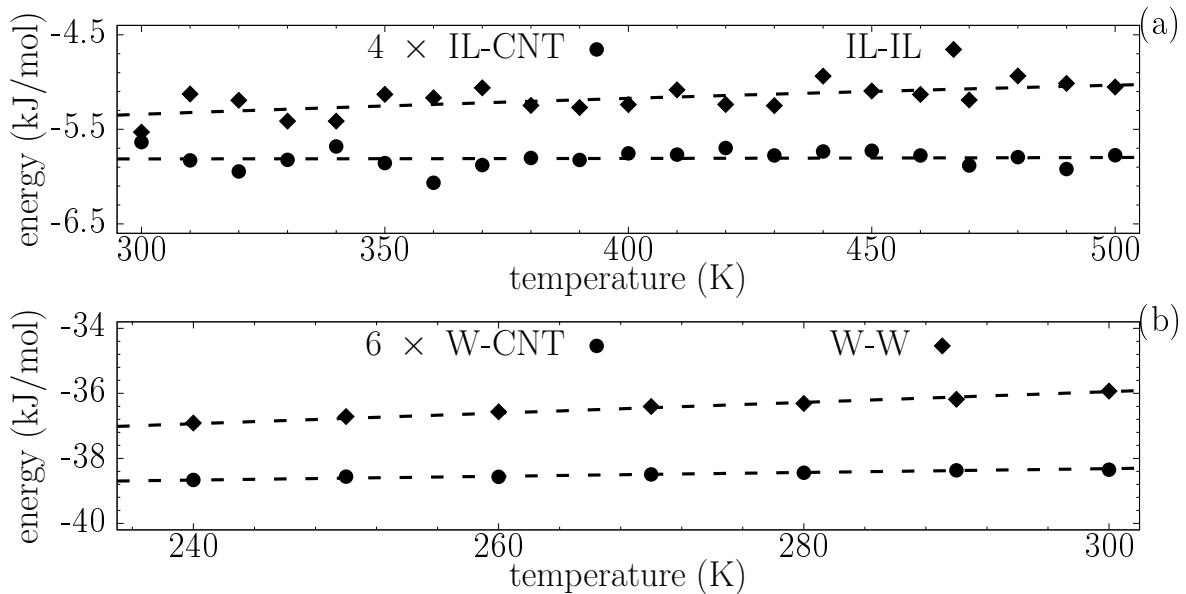

Figure 5. The dependency of interaction potential energy on temperature for (a) IL-CNT and (b) W-CNT models. Dashed lines indicate a linear fit of the data points.

We also simulated water droplets to examine the role of interaction energies between the droplet and nanotube on the thermophoretic forces. We replaced the IL droplet by 850 water molecules (W-CNT) to form a droplet of approximately the same length (l=7 nm) as the IL droplet. Water is modeled with the SPC/E model, with the SHAKE algorithm used to preserve the rigid structure of the water molecules. W-W interactions are known to be stronger than the water W-CNT interaction due to the hydrophobicity of the CNT [29], but the nature of interactions in an IL-CNT system, and their dependence on temperature were yet to be explored. Towards this goal, Figs. 5(a) and (b) show the potential energies at different temperature for IL-CNT and W-CNT models, respectively. These energies are calculated by simulating the systems at a fixed temperatures range from 300 to 500 K, with an increment of 10 K. To avoid evaporation of the water, temperatures between 240 and 300 K are considered for W-CNT system. The IL-CNT and W-CNT interaction energies in Fig. 5 are scaled up by a factor of 4 and 6, respectively, to show them alongside the larger droplet-droplet energies. Not surprisingly, the interaction energies decrease with an increasing temperature.

Thermophoretic forces acting on the droplets can be estimated from the gradient of

the potential energy with respect to temperature. We have followed the same energetic analysis method as Shiomi and Maruyama [29] (for a W-CNT system) to calculate the thermophoretic forces. The potential energy per unit length ϕ' of the droplet is a linear function of z and can thus be represented as $\phi' = az + b$. Hence, the potential energy of the droplet of length L_z can be expressed as in Eq. 1.

$$\phi = \int_0^{L_z} \phi' dz = a\frac{(L_z)^2}{2} + bL_z \tag{1}$$

The droplet is symmetric in both radially and z-direction, such that its centre of mass is located close to the geometric centre z_G of the droplet, i.e., $L_z/2$. The potential energy can thus be expressed as $aL_z z_G + bL_z$ and the force exerted on the particle is expressed in terms of the gradient of potential energy with respect to z.

$$F = -\frac{\partial \phi}{\partial z_G} = -aL_z \tag{2}$$

where 'a' can be deduced from $\phi' = az + b$ as

$$a = \frac{\partial \phi'}{\partial z} = \frac{\partial \phi'}{\partial T}\frac{\partial T}{\partial z} \tag{3}$$

where $\partial T/\partial z$ is the thermal gradient along the CNT. A change in potential energy per atom with respect to change in temperature is obtained from isothermal equilibrium simulations at different temperatures. This gradient term can then be related to Eq. 3 as $L_z \partial \phi'/\partial T = N\partial \phi/\partial T$, where N is the number of IL atoms in the CNT. Note that the sign in front of Eq. 2 was discarded in other studies, since only the magnitude of the force acting on the IL droplet was considered [29]. The thermophoretic force can be expressed as

$$F = -N\frac{\partial T}{\partial z}\frac{\partial \phi}{\partial T} \tag{4}$$

The thermophoretic forces acting on the IL droplet are calculated in two ways: via nonequilibrium simulation and via energetic analysis, by substituting equilibrium simulation results (Fig. 5) into Eq. 4. Fig. 6(a) shows the dependency of the thermophoretic force on the temperature gradients from both approaches. The thermophoretic forces from the nonequilibrium simulations are calculated from the acceleration of the IL droplet due to the applied thermal gradient. These forces are shown as filled black dots in Fig. 6(a). The initial acceleration phase of the IL droplet through the CNT (i.e., phase-I as shown in Fig. 4(a)) is alone considered for the calculations of the thermophoretic force. The error estimates denote the standard error calculated from the 5 individual simulations. The thermophoretic force is found to depend approximately linearly on the applied temperature gradient in the temperature regime considered here. This indicates that simulation results could be extrapolated to smaller thermal gradients for direct comparison with experiments. The change in interaction potential energy with the change in temperature for both IL-CNT and IL-IL is used in Eq. 4 to obtain F_{IL-CNT} and F_{IL-IL}, which is the force on the IL due to IL-CNT
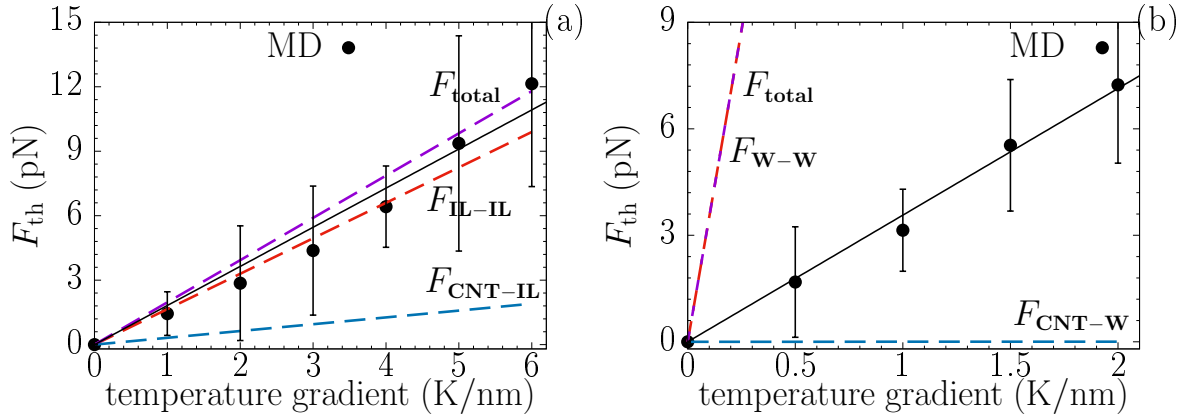
Figure 6. Thermophoretic forces with the temperature gradient for (a) the IL and (b) the water droplets. Filled circles denote results calculated from the acceleration phase in the nonequilibrium simulations. Dashed lines denote the forces calculated from the theoretical approach (Eq. 4), based on the variation in potential energy with temperature in Fig. 5.

and IL-IL interaction potential energies, respectively. Thus, F_{total} is sum of the $F_{\text{IL−CNT}}$ and $F_{\text{IL−IL}}$. The thermophoretic forces calculated from theory and nonequilibrium simulations indicate a near-linear dependence on the thermal gradient, as shown in Fig. 6(a) for the ionic liquid and in Fig. 6(b) for the water droplets. For the IL droplet, a total thermophoretic force of 12 pN is generated on the IL droplet subjected to a thermal gradient of 6 K/nm. For comparison, a strain gradient of 0.4 nm^{-1} can generate a force of about 60 pN on a nanoflake with dimension 1×2.5 nm in the tensile direction [43]. The total thermophoretic force acting on an IL droplet is found to be smaller than on a water droplet of approximately the same size and the same thermal gradient. Although $F_{\text{IL−CNT}} > F_{\text{W−CNT}}$, this is compensated by the much larger liquid-liquid contribution in the case of water, compared to the IL system. It must be noted that the theoretical prediction of the thermophoretic forces overestimates the W-W contribution, consistent with Shiomi and Maruyama [29], while the theoretical prediction for the IL system agrees well with simulation. We also validated the thermophoretic forces by simulating a shorter CNT of diameter 1.38 nm and length 64 nm, with 192 water molecules, similar to the work of Shiomi and Maruyama [29], and found good agreement (data not shown).

The average terminal velocity during the steady phase-III (Fig. 4(a)) is almost proportional to the applied thermal gradient. Figs. 7(a) and (b) show the variation of the average terminal velocity of the IL and water droplets, respectively, as a function of the thermal gradient. The terminal velocity of water under a given thermal gradient was found to be almost independent of the CNT's length and diameter. Another set of simulations is carried out to study the effect of average temperature and nanotube diameter on thermophoretic force and terminal velocity. Five separate simulations were performed with the average CNT temperature ranging from 400 to 650 K while keeping the temperature gradient fixed at 4 K/nm. The thermophoretic force and terminal velocity (Figs. 8(a) and (b)) increase linearly with the increasing average
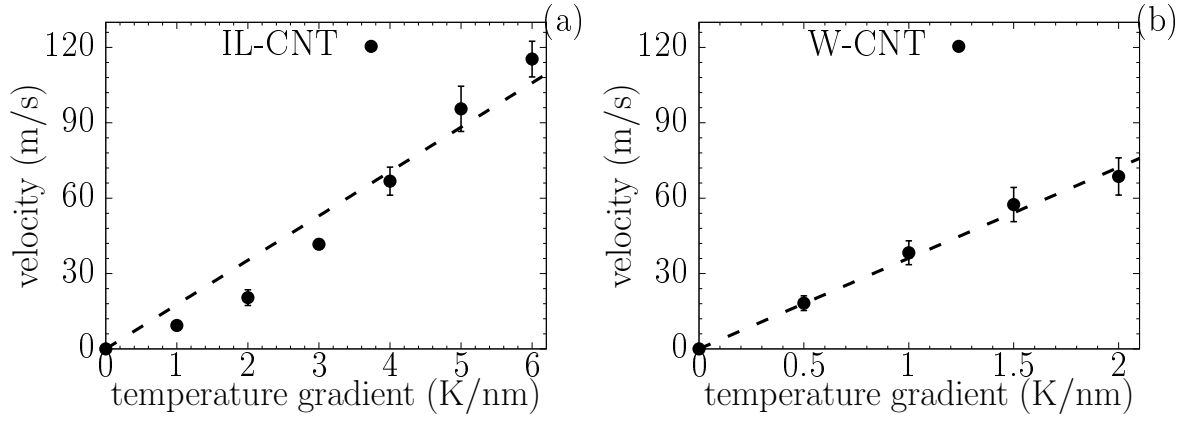
Figure 7. The terminal velocity of the (a) IL and (b) water droplet under an applied temperature gradient. The dashed lines indicate a linear fit of the data.
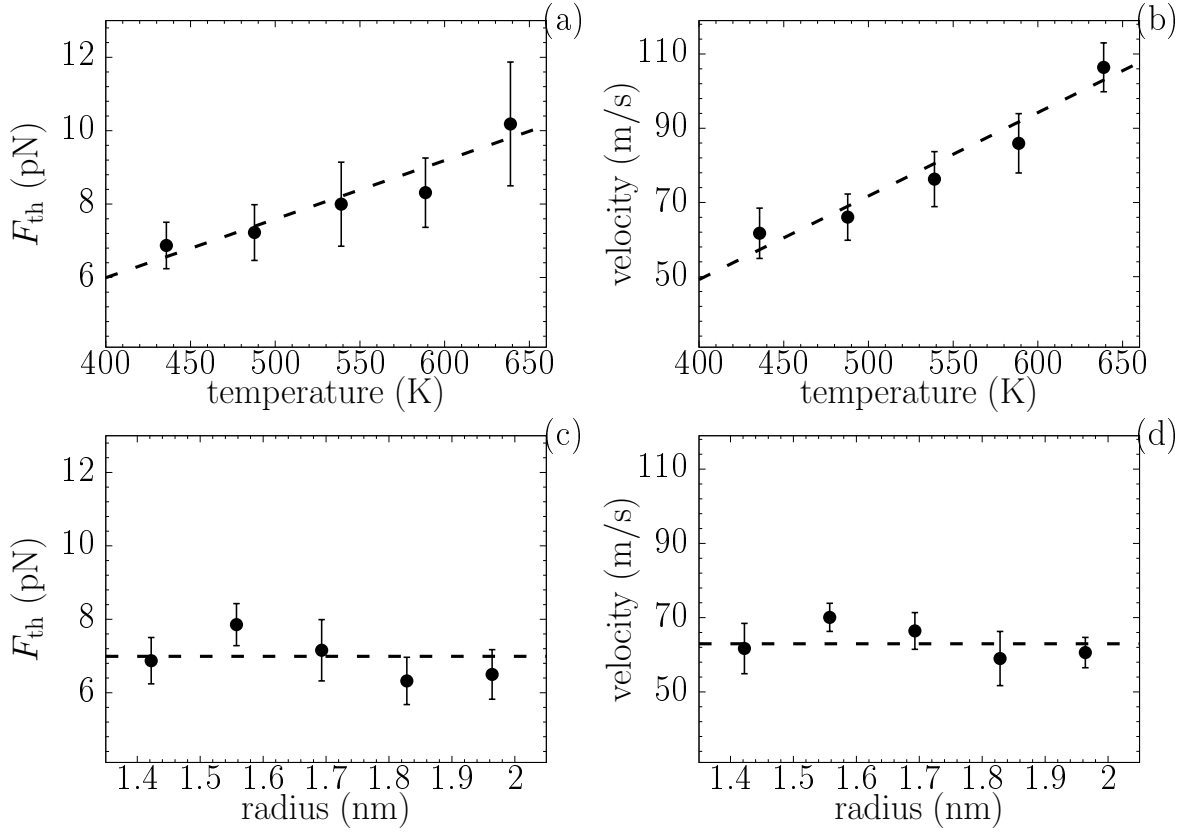
Figure 8. Variation of the thermophoretic force and the terminal velocity as a function of the average system temperature ((a) and (b)) and the radius ((c) and (d)) of the CNT, respectively at a constant thermal gradient of 4 K/nm. The dashed lines indicate a linear fit of the data.

temperature. This contradicts the findings of Hou *et al* [42], a thermophoretic force that was independent of the average CNT temperature. Increasing the nanotube diameter from 2.82 to 3.92 nm (Figs. 8(c) and (d)) has no effect on the thermophoretic force and velocity.

3.1. Moment scaling spectrum

The isothermal diffusion coefficient is measured from 20 ns equilibrium simulations at 300 K. The moment scaling spectrum (MSS) method is used to measure the translational mobility imposed on the fluid by a thermal gradient [45, 46], where the moments of displacement are calculated from the motion of the centre-of-mass position z_{cm} of the IL droplet. Say $z_{\mathrm{cm}}(\mathrm{n})$ be the centre-of-mass position of the IL droplet, where n = 1, 2, 3,.., M, and M is the total number of trajectory points over a temporal resolution of $\Delta t = 2\,\mathrm{ps}$. The moment μ of order ν for a specific frame-shift Δn and for a corresponding time-shift $\delta t = \Delta \mathrm{n} \Delta t$ can be defined as

$$\mu(\Delta \mathrm{n}) = \frac{1}{\mathrm{M} - \Delta \mathrm{n}} \sum_{\mathrm{n}=1}^{\mathrm{M}-\Delta \mathrm{n}} |z_{\mathrm{cm}}(\mathrm{n} + \Delta \mathrm{n}) - z_{\mathrm{cm}}(\mathrm{n})|^{\nu} \tag{5}$$

The mean-squared displacement is a special case of the MSS for order $\nu = 2$. This special case of Eq. 5 is commonly used to calculate the classical self-diffusion coefficient D_2 of fluids. To quantify the diffusion modes of the IL droplets, the moments are calculated for $\nu = 0, 1, 2, .., 6$ and $\Delta \mathrm{n} = 1, 2, .., \mathrm{M} - 1$. The scaling coefficient γ_{ν} for any order can be determined from the slope of the linear least-squares regression profile of $\log(\mu)$ against $\log(\delta t)$. Each moment depends on a time-shift in the power law [45], given by

$$\mu_{\nu}(\delta t) \propto \delta t^{\gamma_{\nu}} \tag{6}$$

The generalized isothermal diffusion coefficient can be determined from

$$D_{\nu} = (2\nu)^{-1}\exp(y_0) \tag{7}$$

where y_0 correspond to value of $\log(\mu)$ at $\log(\delta t)$=0 (Fig. 9(a)).

The MSS is given by the linear relation between the scaling coefficient γ_{ν} and the order ν (Fig. 9(b)) [45], with $\gamma_{\nu=0} = 0$. The slope of the linear profile (S_{MSS}) indicates the type of diffusive motion of the fluid droplet; with slopes of $S_{\mathrm{MSS}} = 0$, 0.5 and 1, representing no diffusive motion, self-similar diffusion and ballistic motion, respectively. These special cases form the boundaries of different diffusive regimes. The region between the slope of 0 and 0.5 is the sub-diffusive regime, observed in the diffusion of confined liquids. The region between the slope of 0.5 and 1 is the super-diffusive regime, found in the case of diffusion with overlaid deterministic drift. If the S_{MSS} profile deviates from a straight trend then it may be due to the weakly self-similar diffusion process. The data in Fig. 9(a) shows larger slopes for $\log(\delta t) < 5$ than for $\log(\delta t) > 5$, suggesting a difference between the short and long-time diffusive behavior of the IL droplet. Fitting only the data in the first 0.15 ns and calculating the corresponding MSS, we find $S_{\mathrm{MSS}} = 0.98$, which denotes a short-time ballistic motion of the IL droplet. For a long time scaling, the MSS profile showed a pronounced kink and its slope changed after 0.2 ns. The dashed red lines in Fig. 9(a) show the least-squares fits to obtain a slope. Thus, for a long-time scaling S_{MSS} is found to be 0.36, which lies in the range of the sub-diffusive regime [46]. The isothermal diffusion coefficient obtained
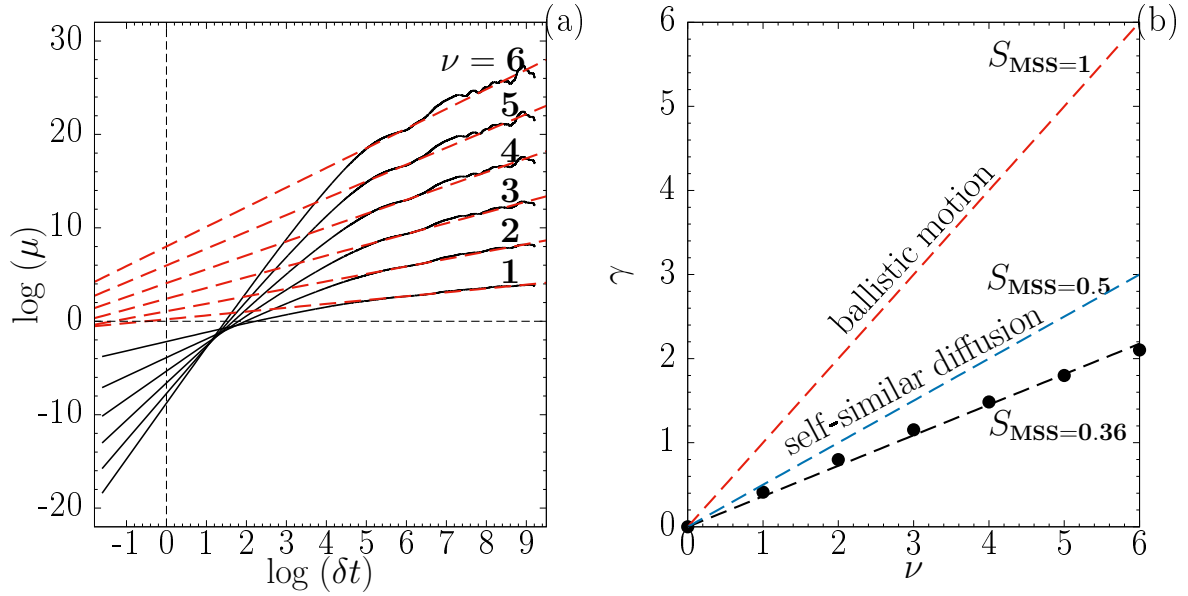
Figure 9. (a) The moments of displacement of the confined IL droplet. The solid black lines show the temporal scaling of the first six moments of displacement. The red dashed lines are the least-squares linear fit to calculate the slopes. (b) The moment scaling spectrum, the black dots indicate the scaling coefficients computed from the linear fits in (a). The black dashed line indicates a linear fit with a slope $S_{MSS} = 0.36$, which falls into the sub-diffusive regime (below the self-similar diffusion line; $0.0 < S_{MSS} < 0.5$).

for the sub-diffusive motion of the IL droplet is estimated to be 0.104 nm^2/ns. Though the obtained isothermal diffusion coefficient is in the range of reported MD studies [37], it is lower than the reported experimental results [21]. This could be related for example to the use of a non-polarizable force field with static partial charges, which can have a substantial influence on the dynamics at the fluid-solid interface.

In nonequilibrium simulations with a temperature gradient, additional diffusion due to the Soret effect will be observed. The Soret coefficient [14, 21] can provide insight into the potential relevance of thermal diffusion. The thermal diffusion coefficient is defined as the ratio of the average velocity of the centre of mass v_{cm} to the applied thermal gradient along the CNT. The ratio of the thermal diffusion coefficient D_t and the isothermal diffusion coefficient D_ν yields the Soret coefficient. From the slope in Fig. 7(a), we have estimated the thermal diffusion coefficient of 17.64 nm^2/(ns K), which corresponds to a Soret coefficient of 169.63 K^{-1}. The estimated Soret coefficient is 2 orders of magnitude larger than the coefficients of the W-CNT system, suggesting that the CNT has more affinity to interact with the IL than with the water. Thus, IL-CNT interactions are not negligible as in the case of the W-CNT system.

4. Conclusion

We have presented a MD simulation study focused on the transport of an ionic liquid (IL) droplet in a carbon nanotube (CNT) subjected to a thermal gradient along its axis. The droplet was found to drift along the axis of the CNT against the direction of the imposed thermal gradient, towards lower temperature region. The measured thermophoretic force and the average terminal velocity from nonequilibrium MD simulations were found to scale linearly with the thermal gradient, suggesting that results could be extrapolated down to lower thermal gradient for a direct comparison to experiments. A terminal velocity as high as 155 m/s was reached for the thermal gradient 6 K/nm. The energetic analysis for the IL-CNT system has shown that the transport of the droplet depends on both IL-CNT (interfacial) and IL-IL interaction potential energies. An increase in the average system temperature (while keeping the thermal gradient fixed) resulted in a larger fluid-solid interaction energy, which caused an increase in the thermophoretic driving force. The thermophoretic force thus depends on the average temperature and on the temperature gradient, while no dependence on the tube diameter was found.

Additional simulations with water were carried out to investigate the nature of droplet on the thermophoretic motion. For the water-CNT systems, potential energies of droplet-droplet interactions dominate the droplet-nanotube interaction, in contrast to the IL-CNT system. A moment scaling spectrum analysis showed that the isothermal diffusion coefficient of the confined IL droplet falls into the sub-diffusion regime, while the motion of the water droplet was self-diffusive. The corresponding Soret coefficient and energetic analysis suggested that the CNT shows more affinity for interaction with the IL droplet than with the water droplet. The strong connection between the IL and the CNT, combined with the potential energy gradient along the tube length, suggest that thermophoresis can be suitable for the transport of IL through a CNT. Our findings illustrated the potential of using thermal gradients to accurately control IL transport in confinement. This can benefit the use of IL as heat transfer agent in solar cells and as an electrolyte in supercapacitors for energy storage applications.

References

[1] Reto B. Schoch, Jongyoon Han, and Philippe Renaud. Transport phenomena in nanofluidics. *Rev. Mod. Phys.*, 80:839–883, 2008.

[2] Napoli, M. and Eijkel, J. C. T. and Pennathur, S. Nanofluidic technology for biomolecule applications: a critical review. *Lab Chip*, 10(8):957-985, 2010.

[3] Peter J. F. Harris. *Carbon Nanotubes and Related Structures.* Cambridge University Press, 1999.

[4] M. S. Sansom and P. C. Biggin. Water at the nanoscale. *Nature*, 414(6860):156–159, 2001.

[5] Duy Tho Pham, Tae Hoon Lee, Dinh Hoa Luong, Fei Yao, Arunabha Ghosh, and Viet Thong Le. Carbon Nanotube-Bridged Graphene 3D Building Blocks for Ultrafast Compact Supercapacitors. *ACS Nano*, 9(2):2018–2027, 2015.

[6] Stefan Duhr and Dieter Braun. Why molecules move along a temperature gradient. *Proceedings of the National Academy of Sciences of the United States of America*, 103(52):19678–82, 2006.

[7] J. F. Dutrieux, J. K. Platten, G. Chavepeyer, and M. M. Bou-Ali. On the measurement of positive soret coefficients. *Journal of Physical Chemistry B*, 106(23):6104–6114, 2002.

[8] Joe Francis Thekkethala and Sarith P. Sathian. Thermal transpiration through single walled carbon nanotubes and graphene channels. *The Journal of Chemical Physics*, 139, 174712, 2013

[9] Tuan Vo-Dinh, Brian M. Cullum, and David L. Stokes. Nanosensors and biochips: Frontiers in biomolecular diagnostics. *Sensors and Actuators, B: Chemical*, 74(1-3):2–11, 2001.

[10] Remco Hartkamp, Bertrand Siboulet, Jean-Francois Dufreche, and Benoit Coasne. Ion-specific adsorption and electroosmosis in charged amorphous porous silica. *Phys. Chem. Chem. Phys.*, 17:24683–24695, 2015.

[11] Jijie J. Zhou, Flavio Noca, and Morteza Gharib. Flow conveying and diagnosis with carbon nanotube arrays. *Nanotechnology*, 17(19):4845–4853, 2006.

[12] Jason K. Holt, Hyung Gyu Park, Yinmin Wang, Michael Stadermann, Alexander B. Artyukhin, Costas P Grigoropoulos, Aleksandr Noy, and Olgica Bakajin. Sub-2-Nanometer Carbon Nanotubes. *Science*, 312(May):1034–1038, 2006.

[13] Ludwig C. Diffusion zwischen ungleich erwrmten Orten gleich zusammengesetzter Lsungen [Diffusion of homogeneous fluids between regions of different temperature]. *Sitzungsbericht Kaiser Akad Wiss, ed Braunmller W (Mathem-Naturwiss Cl, Vienna)*, 65:539, 1856.

[14] Ch. Soret. Sur L'tat D'quilibre Que Prend au Point de Vue de sa Concentration une Dissolution Saline Primitivement Homohne Dont Deux Parties Sont Portes des Tempratures Diffrentes. *Annales de chimie et de physique*, 22:293297, 1881.

[15] J. C. Maxwell. On stresses in rarified gases arising from inequalities of temperature. *Philos. Trans. R. Soc.*, 11(January):231–256, 1879.

[16] Yoshio Sone. Flows Induced by Temperature Fields in a Rarefied Gas and their Ghost Effect on the Behavior of a Gas in the Continuum Limit. *Annual Review of Fluid Mechanics*, 32(1):779–811, 2000.

[17] F. Zheng. Thermophoresis of spherical and non-spherical particles: a review of theories and experiments. *Advances in Colloid and Interface Science*, 97(13):255 – 278, 2002.

[18] T. L. Ibbs. The Experimental Development of Thermal Diffusion. *Physica IV*, 10:1133–1140, 1937.

[19] T. L. Ibbs and S. Chapman. Some experiments on thermal diffusion. *Proceedings of the Royal Society of London A: Mathematical, Physical and Engineering Sciences*, 99(700):385–397, 1921.

[20] A. S. Fedorov and A. F. Sadreev. Thermoactivated transport of molecules H 2 in narrow single-wall carbon nanotubes. *European Physical Journal B*, 69(3):363–368, 2009.

[21] Harvey A. Zambrano, Jens H. Walther, Petros Koumoutsakos, and Ivo F. Sbalzarini. Thermophoretic motion of water nanodroplets confined inside carbon nanotubes. *Nano Letters*, 9(1):66–71, 2009.

[22] Philipp A. E. Schoen, Jens H. Walther, Salvatore Arcidiacono, Dimos Poulikakos, and Petros Koumoutsakos. Nanoparticle traffic on helical tracks: Thermophoretic mass transport through carbon nanotubes. *Nano Letters*, 6(9):1910–1917, 2006.

[23] Ning Wei, Hui-Qiong Wang, and Jin-Cheng Zheng. Nanoparticle manipulation by thermal gradient. *Nanoscale research letters*, 7(1):154, 2012.

[24] Amelia Barreiro, Riccardo Rurali, Eduardo R. Hernandez, Joel Moser, Thomas Pichler, László Forró, and Adrian Bachtold. Subnanometer motion of cargoes driven by thermal gradients along carbon nanotubes. *Science*, 320(5877):775–778, 2008.

[25] Hiroshi Somada, Kaori Hirahara, Seiji Akita, and Yoshikazu Nakayama. A Molecular Linear Motor Consisting of Carbon Nanotubes. *Nano Letters*, 9:62–65, 2009.

[26] Z. Y. Guo, Q. W. Hou, and B. Y. Cao. A Novel Thermal Driving Force for Nanodevices. *Journal of Heat Transfer*, 134(May):51010, 2012.

[27] Zhengrong Guo, Tienchong Chang, Xingming Guo, and Huajian Gao. Mechanics of thermophoretic and thermally induced edge forces in carbon nanotube nanodevices. *Journal of the Mechanics and Physics of Solids*, 60(9):1676–1687, 2012.

[28] Prathamesh M. Shenai, Zhiping Xu, and Yang Zhao. Thermal-gradient-induced interaction energy ramp and actuation of relative axial motion in short-sleeved double-walled carbon nanotubes.

Nanotechnology, 22(48):485702, 2011.

[29] J. Shiomi and S. Maruyama. Water transport inside a single-walled carbon nanotube driven by a temperature gradient. *Nanotechnology*, 20(Md):055708, 2009.

[30] R. Rurali and E. R. Hernandez. Thermally induced directed motion of fullerene clusters encapsulated in carbon nanotubes. *Chemical Physics Letters*, 497(1-3):62–65, 2010.

[31] Suojiang Zhang, Ning Sun, Xuezhong He, Xingmeo Lu and Xiangping Zhang. Physical properties of Ionic liquids: Database and Evaluation. *Physical Properties of Ionic Liquids: Database and Evaluation*, 35(4):1475–1517, 2006.

[32] Thomas Welton. Room-temperature ionic liquids. solvents for synthesis and catalysis. *Chemical Reviews*, 99(8):2071–2084, 1999. PMID: 11849019.

[33] Sang-Young Lee, Hyun Hang Yong, Young Joo Lee, Seok Koo Kim, and Soonho Ahn. Two-cation competition in ionic-liquid-modified electrolytes for lithium ion batteries. *The Journal of Physical Chemistry B*, 109(28):13663–13667, 2005. PMID: 16852712.

[34] Roberto F. de Souza, Janine C. Padilha, Reinaldo S. Gonalves, and Jairton Dupont. Room temperature dialkylimidazolium ionic liquid-based fuel cells. *Electrochemistry Communications*, 5(8):728 – 731, 2003.

[35] N. Papageorgiou, Y. Athanassov, M. Armand, P. Bonhote, H. Pettersson, A. Azam, and M. Grtzel. The performance and stability of ambient temperature molten salts for solar cell applications. *Journal of The Electrochemical Society*, 143(10):3099–3108, 1996.

[36] Steve Plimpton. Fast parallel algorithms for short-range molecular dynamics. *Journal of Computational Physics*, 117(1):1 – 19, 1995.

[37] Jose N. Canongia Lopes, Agilio A. H. Padua, and Karina Shimizu. Molecular Force Field for Ionic Liquids IV: Trialkylimidazolium and Alkoxycarbonyl-Imidazolium Cations; Alkylsulfonate and Alkylsulfate Anions. *Journal of Physical Chemistry B*, 112:5039–5046, 2008.

[38] E J Maginn. Molecular simulation of ionic liquids: current status and future opportunities. *Journal of Physics: Condensed Matter*, 21(37):373101, 2009.

[39] Donald W. Brenner, Olga A. Shenderova, Judith A. Harrison, Steven J. Stuart, Boris Ni, and Susan B. Sinnott. A second-generation reactive empirical bond order (rebo) potential energy expression for hydrocarbons. *Journal of Physics: Condensed Matter*, 14(4):783, 2002.

[40] H. A. Zambrano, J. H. Walther, and R. L. Jaffe. Thermally driven molecular linear motors: A molecular dynamics study. *Journal of Chemical Physics*, 131(24):10–13, 2009.

[41] Ruijuan Qiao, Qi Wang, and Yingchun Liu. Abnormal transport properties of Argon confined in carbon nanotube driven by a temperature gradient. *Chemical Physics Letters*, 597:143–147, 2014.

[42] Quan-Wen Hou, Bing-Yang Cao, and Zeng-Yuan Guo. Thermal gradient induced actuation in double-walled carbon nanotubes. *Nanotechnology*, 20(49):495503, 2009.

[43] Chao Wang, and Shaohua Chen. Motion Driven by Strain Gradient Fields. *Scientific Reports*, 5:13675, 2015.

[44] Jeffrey Comer, James C. Gumbart, Jrme Hnin, Tony Lelivre, Andrew Pohorille, and Christophe Chipot. The adaptive biasing force method: Everything you always wanted to know but were afraid to ask. *The Journal of Physical Chemistry B*, 119(3):1129–1151, 2015. PMID: 25247823.

[45] R. Ferrari, A. J. Manfroi, and W. R. Young. Strongly and weakly self-similar diffusion. *Physica D: Nonlinear Phenomena*, 154(1-2):111–137, 2001.

[46] I. F. Sbalzarini and P. Koumoutsakos. Feature point tracking and trajectory analysis for video imaging in cell biology. *Journal of Structural Biology*, 151(2):182–195, 2005.